

Research Paper

Nrf2 signaling and inflammation are key events in physical plasma-spurred wound healing

Anke Schmidt¹✉, Thomas von Woedtke^{1,2}, Brigitte Vollmar³, Sybille Hasse¹, Sander Bekeschus¹

1. Leibniz-Institute for Plasma Science and Technology (INP Greifswald), Plasma Life Science and ZIK *plasmatis*, Felix-Hausdorff-Str. 2, 17489 Greifswald, Germany
2. Department of Hygiene and Environmental Medicine, University Medicine Greifswald, 17475 Greifswald, Germany
3. Institute for Experimental Surgery, University of Rostock, Schillingallee 69a, 18057 Rostock, Germany

✉ Corresponding author: Anke Schmidt, Leibniz-Institute for Plasma Science and Technology, Felix-Hausdorff-Str. 2, 17489 Greifswald, Germany, Phone: +49 3834 5543958, Fax: +49 3834 554301, Email: anke.schmidt@inp-greifswald.de

© Ivyspring International Publisher. This is an open access article distributed under the terms of the Creative Commons Attribution (CC BY-NC) license (<https://creativecommons.org/licenses/by-nc/4.0/>). See <http://ivyspring.com/terms> for full terms and conditions.

Received: 2018.09.06; Accepted: 2019.01.02; Published: 2019.01.30

Abstract

Wound healing is strongly associated with the presence of a balanced content of reactive species in which oxygen-dependent, redox-sensitive signaling represents an essential step in the healing cascade. Numerous studies have demonstrated that cold physical plasma supports wound healing due to its ability to deliver a beneficial mixture of reactive species directly to the cells.

Methods: We described a preclinical proof-of-principle-concept of cold plasma use in a dermal, full-thickness wound model in immunocompetent SKH1 mice. Quantitative PCR, Western blot analysis, immunohistochemistry and immunofluorescence were performed to evaluate the expression and cellular translocation of essential targets of Nrf2 and p53 signaling as well as immunomodulatory and angiogenic factors. Apoptosis and proliferation were detected using TUNEL assay and Ki67 staining, respectively. Cytokine levels in serum were measured using bead-based multiplex cytokine analysis. Epidermal keratinocytes and dermal fibroblasts were isolated from mouse skin to perform functional knockdown experiments. Intravital fluorescence analysis was used to illustrate and quantified microvascular features.

Results: Plasma exerted significant effects on wound healing in mice, including the promotion of granulation and reepithelialization as a consequence of the migration of skin cells, the balance of antioxidant and inflammatory response, and the early induction of macrophage and neutrophil recruitment to the wound sites. Moreover, through an early and local plasma-induced p53 inhibition with a concomitant stimulation of proliferation, the upregulation of angiogenic factors, and an increased outgrowth of new vessels, our findings explain why dermal skin repair is accelerated. The cellular redox homeostasis was maintained and cells were defended from damage by a strong modulation of the nuclear E2-related factor (Nrf2) pathway and redox-sensitive p53 signaling.

Conclusions: Although acute wound healing is non-problematic, the pathways highlighted that mainly the activation of Nrf2 signaling is a promising strategy for the clinical use of cold plasma in chronic wound healing.

Key words: Nrf2; p53; plasma medicine; reactive species; redox regulation; wound healing

Introduction

Physiological tissue repair is orchestrated by the interaction of macrophages, platelets, neutrophils, fibroblasts, keratinocytes, and endothelial cells, and their activation of regulatory pathways that promote healing [1]. The major phases of wound healing –

inflammation, formation of granulation tissue, and reepithelialization, together with tissue remodeling – require the finely tuned regulation of cellular dynamics and protein expression. The third, and sometimes underappreciated, pillar in wound healing

is redox control. The endogenous generation of oxidants leads to reversible oxidative modifications on thiol groups, which contribute to physiological or pathological stages of wound healing [2]. In chronic wounds, there is evidence of a misbalanced cellular redox level [3, 4]. This modulates apoptosis [5], decreases the expression of angiogenic growth factors [6], impairs neovascularization [7], and prolongs inflammation [8], for instance, in diabetic wounds [9]. Several downstream targets of the transcription factor p53 contribute to the regulation of cellular reactive species levels and play a major role in the cellular signaling network [10]. Depending on species concentration, p53 activates both pro-oxidants promoting autophagy and antioxidant responses [11] to regulate cell repair, senescence, DNA damage recognition, proliferation, and migration [12]. Several antioxidants and enzymes are partially sufficient to stimulate the nuclear erythroid-related factor 2 (Nrf2) pathway in skin, leading to an increase in glutathione content, thereby improving the quality of the skin [13] and healing responses [14]. Hence, wound healing is subject to redox control [15].

Cold physical plasma is a partially ionized gas and a potent source of a multitude of gaseous reactive oxygen species (ROS) and nitrogen species (RNS) [16]. Consequently, cold plasma modulates numerous cellular processes related to redox signaling and may be useful for targeting a plethora of specific, wound healing-related pathways [17, 18]. In addition to several rodent studies [19–22], patients with chronic wounds and ulcers have also benefited from clinical plasma therapy [23, 24].

Notwithstanding the clinical success of exogenous reactive species therapy using cold plasmas, there is limited direct evidence and molecular understanding as to how reactive species may be used to trigger the appropriate redox signaling pathways to improve healing. As such, we utilized a murine full-thickness ear incision model to investigate early and late stage effects of plasma treatment in wounds. A number of targets were identified from gene and protein expression profiling that concomitantly regulated accelerated wound healing. Nrf2 and p53 signaling pathways were shown to be key factors in these responses.

Materials and Methods

Animals and wounding

A total of 113 SKH1-hr hairless immunocompetent mice (Charles River Laboratories, Sulzfeld, Germany) were housed under standard conditions in an animal facility (Medical Faculty of University of Rostock, Rostock, Germany). Wounding

on both ears using a microscissor was performed, as previously described by removing of upper epidermal and dermal layer [22]. The area of the full-thickness dermal wound was ~ 3 mm². The present immunocompetent ear wound model is well-suited as a model system of acute physiological wound healing in humans due to the predominantly reepithelialization by migration and the absence of muscle contraction [12, 25–27]. All experiments were approved by the local ethics committee according to the guidelines for care and use of laboratory animals (7221.3-1-013/14 and 044/16) and to the NIH Guide for the Care and Use of Laboratory Animals.

Exposure to cold physical plasma and wound closure measurements

An atmospheric pressure argon plasma jet (*kINPen*; neoplas tools, Greifswald, Germany) was used, which ionized a flow (5 standard liters per minute) of argon gas (purity 99.9999; Air Liquide, Krefeld, Germany) at 1 MHz. Plasma treatment of wounds was performed using the tip of the plasma effluent at a constant distance of 8 mm using a autoclavable spacer. Ear wounds were treated for 3 s or 20 s or with hydrogen peroxide (H₂O₂, 1 mM; Sigma-Aldrich, Traunstein, Germany). Treatment was administered three times per week with plasma or a placebo (argon gas alone) or were left untreated (ctrl) over 6 (thrice in total; only females) or 14 (six times in total) consecutive days (**Figure S1**). An overview of experimental design including the number of animals in all experimental groups is given (**Table 1**). The study protocol and number of animals were in part specified by the local ethics committee. Reepithelialization and wound closure were studied by stereomicroscopy (Leica Microsystems, Wetzlar, Germany) on the day of wounding (d0) and every third day after thereafter.

Homogenization of ear tissue and expression analysis

Homogenization. For expression analysis, tissue from right ears was collected at day 6 and 15. Briefly, fresh tissues from ears were removed, snap-frozen in liquid nitrogen, and stored at -80°C . Homogenization was performed in RNA lysis buffer (Bio&Sell, Feucht, Germany) for gene expression analysis, or in RIPA buffer containing protease and phosphatase inhibitors (cOmplete Mini, phosSTOP, PMSF, Sigma-Aldrich, Traunstein, Germany) for protein validation experiments using a FastPrep-24 5G homogenizator (MP biomedical, Heidelberg, Germany).

mRNA analysis. Total RNA was purified according to the manufacturer's instructions (Bio&Sell, Feucht, Germany) and RNA quality was

evaluated using Bioanalyzer 2100 (Agilent, Santa Clara, CA, USA). For quantification of mRNAs by quantitative PCR (qPCR), 1 µg of RNA was transcribed into cDNA and qPCR was conducted in duplicate using SYBR Green I Master (Roche Diagnostics, Basel, Switzerland). Gene specific primers were used from BioTez (Berlin, Germany) as shown (Table S1). The housekeeping gene *GAPDH*, whose expression was unaffected by plasma, was used as an internal control for normalization. Gene expression was analyzed using the $\Delta\Delta CT$ method.

Protein analysis. Protein targets were validated on the basis of their significance within the main cellular responses. These included molecules of the Nrf2-pathway (e.g. HO-1 and Nqo1) as well as antioxidative response targets such as Sod1, Cat, Trxr1, Prdx6, KGF, Akt, and phospho-Akt (p-Akt). *GAPDH* served as housekeeping protein (all Cell signaling, Frankfurt/Main, Germany). Western blot analysis was performed using WES according to the manufacturer's instructions. Band intensities were quantified using ImageQuantTL Software (GE Healthcare, München, Germany), and expressed as fold change compared to the corresponding control. Blood serum was collected retrobulbarly in EDTA-tubes at days 0 and 15, centrifuged, and stored until use at -80 °C. Cytokine levels in serum were measured using bead-based multiplex cytokine analysis (BioLegend, San Diego, USA) according to the vendor's protocol, acquired on a CytoFlex S flow cytometer (Beckman-Coulter, Indianapolis, IN, USA) and analyzed using LegendPlex software 8.0 (VigineTech, San Diego, CA, USA).

Cell culture and knockdown of NRF2 and KEAP1 by short interfering RNA (siRNA)

To evaluate the effect of cold plasma on cellular translocation of Nrf2, dermal fibroblasts and epidermal keratinocytes (Figure S2A) were isolated from SKH1 skin (n = 6) and cultivated over 14 days in a keratinocytes or fibroblasts EMEM medium (PromoCell, Heidelberg, Germany) at 37°C with 5% CO₂ in a humidified incubator.

In knockdown experiments, siRNAs (1 µg) targeting Nrf2 and Keap1 were transfected into keratinocytes using Effectene (Qiagen, Hilden, Germany) transfection reagent according to the respective protocol [28]. Knockdown of both genes was validated by semi-quantitative PCR (Figure S2B) and by qPCR. Seventy-two hours after transfection, cells were plasma-treated for 60 s and incubated for 20 min prior to down-stream investigations. A non-targeting siRNA (scrRNA) was used as a negative control, and a GFP plasmid was employed to determine transfection efficacy (Figure S2C).

Histological and immunohistochemical analyses

On days 6 and 15, wound regions of the left ears and organs such as lungs, brains, spleens, and livers were collected and fixed in 4 % paraformaldehyde (Sigma-Aldrich, Traunstein, Germany) overnight. Paraffin blocks were cut into 5 µm-sections using a microtome to retrieve tissue sections that were stained with hematoxylin and eosin (H&E; Carl-Roth, Karlsruhe, Germany). Collagen fibers were visualized using picosirius red (Direktrot 80, Sigma-Aldrich, Traunstein, Germany) as described [29].

Identification of myeloid cells. Macrophages (including Kupffer cells) were labeled with an anti-F4/80 antibody (#14-4801; Affymetrix, Frankfurt/Main, Germany). In wounds and spleens, neutrophils were identified with an anti-Ly6G antibody (#14-5931; Affymetrix, Frankfurt/Main, Germany). After washing, sections were incubated with an immuno-peroxidase polymer (N-Histofine staining reagent; Medac, Germany) or with a secondary antibody coupled to an Alexa-Fluor 594 dye (Life Technologies, Darmstadt, Germany).

Detection of proliferation and apoptosis. Ki67 labeling of proliferating cells (IHC-00375, Biomol, Hamburg, Germany) was performed in paraffin-embedded ear tissue sections according to the vendor's instructions. Terminal deoxynucleotidyl transferase (TdT) dUTP Nick-End Labeling (TUNEL) assay (Roche, Basel, Switzerland) was used to detect late apoptotic cells known to have fragmented DNA. In both stainings, Hoechst 33243 (Sigma-Aldrich, Traunstein, Germany) was used to counterstain nuclei.

Microscopy and data evaluation. Stained sections were mounted onto glass microscope slides using a mounting medium (VectaShield; Biozol, Eching, Germany) prior to analysis using an Axio Observer Z.1 (Zeiss, Jena, Germany). At least three to five fields of view (FOV) were analyzed per animal and ear wound. As a reference point, a standard 20 × microscope objective has a resolution of ~0.8 µm and an FOV of ~5 × 10⁻² mm² and was used for our analyses [30]. Proliferative (Ki67 positive, red), and apoptotic (TUNEL positive, green) cells were counted, and the ratio between green or red nuclei over the total number of nuclei (Hoechst, blue) was calculated in three directly neighboring FOV within the wound granulation tissue. Macrophages (F4/80 positive) and neutrophils (Ly6G positive) were quantified as density and are given as n/n of Hoechst in a FOV (number of red cells / number of Hoechst cells in the same area). All quantification were analyzed using Fiji macro collection for ImageJ software. By using qualitative scores between 1 to 5 (1 = none, 2 =

minimal, 3 = moderate, 4 = pronounced, 5 = high/complete) collagen patterns, inflammation, granulation, angiogenesis, and apoptosis were analyzed in paraffin-embedded sections within three to five FOV (Table 2).

Intravital fluorescence analysis of blood vessel formation

After retrobulbar injection of 0.1 mL phosphate-buffer saline containing 2% fluorescein isothiocyanate (FITC)-labeled dextran (150 kDa; Sigma Chemicals, Deisenhofen, Germany) for the visualization of blood vessels, the angiogenetic effects of plasma treatment (only for 20 s) were analyzed in wound ear regions on days 6 and 15. An intravital fluorescence epi-illumination microscope (IVM, Axiotech Vario; Zeiss, Jena, Germany) was used and a qualitative scoring of newly formed blood vessels was completed. For quantitative measurements of angiogenesis and neovascularization, FITC-dextran stained microvessels were analyzed with IVM (Figure 6AIII). Functional microvessel density (FMD), defined as the total length of microvessels per FOV (cm/cm²), as well as radial and circular capillary diameter were assessed in up to three images using ImageJ software [26, 31].

Statistical analysis

All experiments were done with tissue of 3-9 animals per group. *In vitro* assays were repeated three times independently. Values give mean + S.D. If not indicated otherwise, and data were statistically compared with *p* values indicated by **p*<0.05, ***p*<0.01, or ****p*<0.001. Graphics and statistical analysis were performed with *prism* 7.04 (GraphPad software, San Diego, CA, USA) using unpaired Student's *t* test or one-way ANOVA (for angiogenesis).

Results

Cold plasma promoted wound closure depending on treatment time

We examined the cold plasma's potential to promote reepithelialization in our mouse model of dermal full-thickness ear wounds (Figure S1A-B). Mice either received treatments three-times per week or were left untreated (ctrl) over 6 and 14 consecutive days after wounding (Table 1). Wound closure kinetics suggested improved healing in the plasma-treated wounds compared to the non-treated wounds (Figure 1A-B). Quantitative analysis showed significantly accelerated wound closure beginning on day 3 in females (right) and on day 6 in males (left, Figure 1C). A near-complete reepithelialization (92-98 %) was achieved on day 12 without scar

formation (Figure S1C). On day 15 post wounding, the thickness of the newly formed epidermal layer was comparable in all experimental groups (Figure 1D), suggesting normal, physiological healing among all groups. Placebo treatment with argon gas (data not shown) and hydrogen peroxide controls were similar in range as untreated controls (Table S2).

Table 1: Overview of experimental groups, treatment regimes, time of sacrifice after wounding, and gender (d, day; s, seconds). Primary cells (e.g., keratinocytes and fibroblasts) were isolated from the skin of ten males and cultivated over four weeks as described in material and methods.

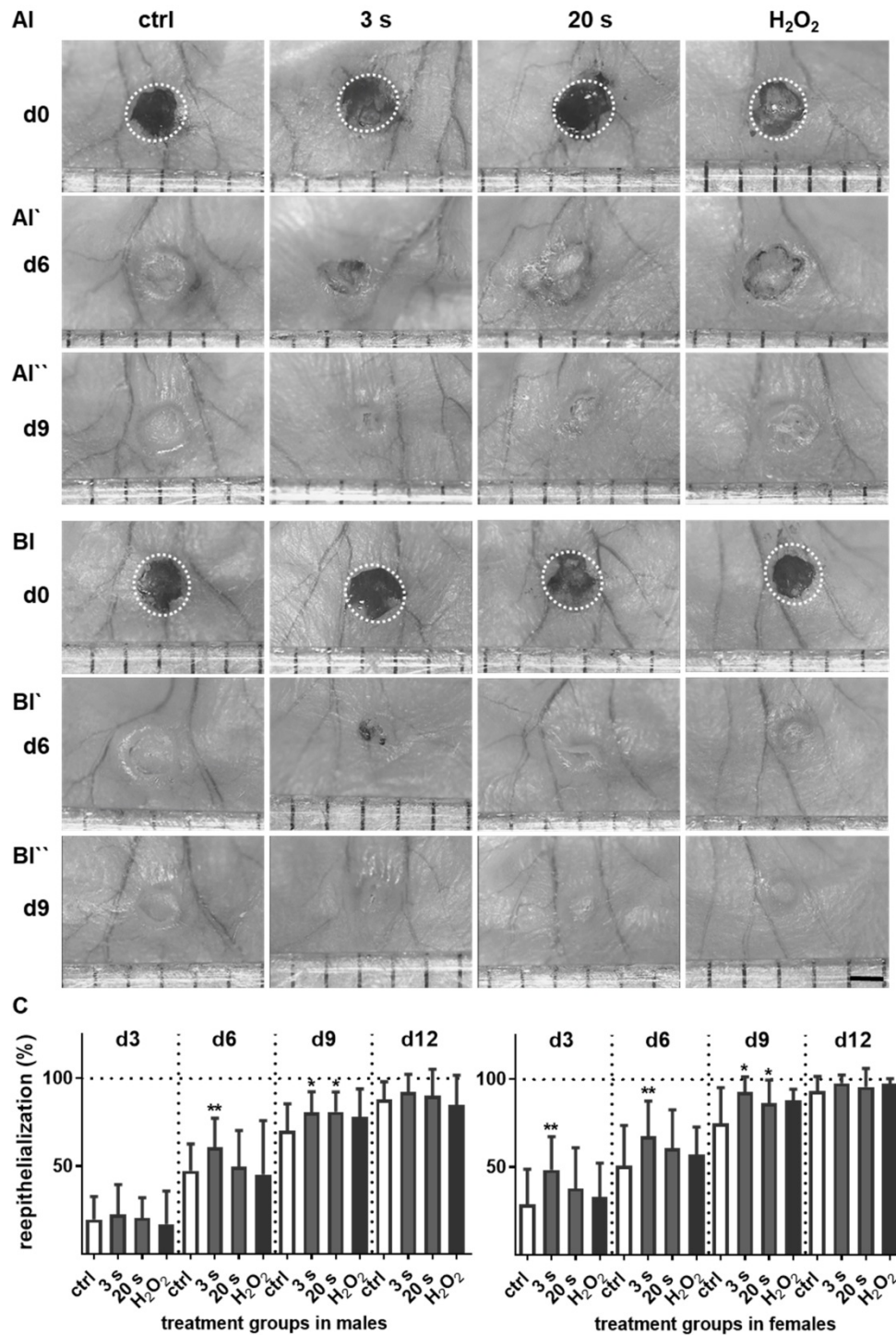
Groups	Day (d) of tissue collection	Treatment regime	Male♂	Female♀
3 s plasma	d3	3 s for two times (d0, d3)	-	3
ctrl		0 s	-	3
3 s plasma	d6	3 s (3x on d0, d3, d6)	-	4
20 s plasma		20 s (3x on d0, d3, d6)	-	3
ctrl		0 s	10	11
3 s plasma	d15	every 3 rd d over 14 d (6x)	10	13
20 s plasma		every 3 rd d over 14 d (6x)	9	12
H ₂ O ₂ (1 mM)	d15	every 3 rd d over 14 d (6x)	9	8
argon (0, 3, 20 s)	d15	every 3 rd d over 14 d (6x)	-	9
primary cells	-	-	6	3

Healing responses were examined by scoring of five parameters (Table 2) that include tissue collagen patterns (distribution, fiber orientation, early and mature collagen, amount of collagen), inflammation (inflammatory infiltrate), granulation (granulation tissue, cell accumulation, cell migration), angiogenesis (blood vessel formation, vascularization), and apoptosis (blebbing, shrinking, condensation). Each of the five parameters was graded from 1 (worst regarding healing) to 5 (best regarding healing) on days 6 and 15, and included the following features for each score: lack of healing response, absence of collagen fibers, high inflammatory infiltrate, absence of granulation tissue, no blood vessel formation and apparent apoptosis (**score 1**); thin epithelialization, scanty collagen fiber formation and granulation, marked inflammation with presence of immune cells, mild microvessel formation, and pronounced apoptosis (**score 2**); moderate collagen deposition, granulation, inflammation, microvessel formation, and apoptosis (**score 3**); pronounced collagen deposition, mild inflammation, profound granulation and blood vessel formation, and mild apoptosis (**score 4**); and complete wound closure with plenty of collagen fibers, absence of or minimal inflammation, profound tissue granulation, apparent angiogenesis, and lack of apoptosis (**score 5**).

Overshooting collagen is the main reason for fibrosis [32]. At the early time point (d6), picosirius red (PSR)-stained fibers were increased in all plasma-treated groups (Figure 1D, right diagram). Although the accumulation of collagen fibers

appeared regularly ordered with multiple orientations within the dermal layers (**Figure S1D**), evaluation on day 15 revealed a significant increase (score 3.9) especially for 20 s of plasma treatment (**Figure 1D**, left and middle diagram). For tissue granulation and inflammatory infiltrate, no significant differences were observed on day 15 in contrast to day 6. The mean inflammation score was 4.8 (3 s) and 4.4 (20 s) in plasma-treated groups. Based on evaluation of cell accumulation and cell migration the mean granulation score was 2.5 for both plasma-treated

groups. Apoptosis was less pronounced upon plasma treatment (score 2.9 for 3 s and 2.7 for 20 s) compared to the control group (score 1) on day 6. Importantly, formation of new blood microvessels (microvessel outgrowth) was marginally but significantly increased in plasma-treated animals with a score of 3.4 (3 s) and 3.1 (20 s) in contrast to controls (2.1). The majority of features for plasma-treated animals scored significantly better compared to controls as shown in Table 2 (asterisks).



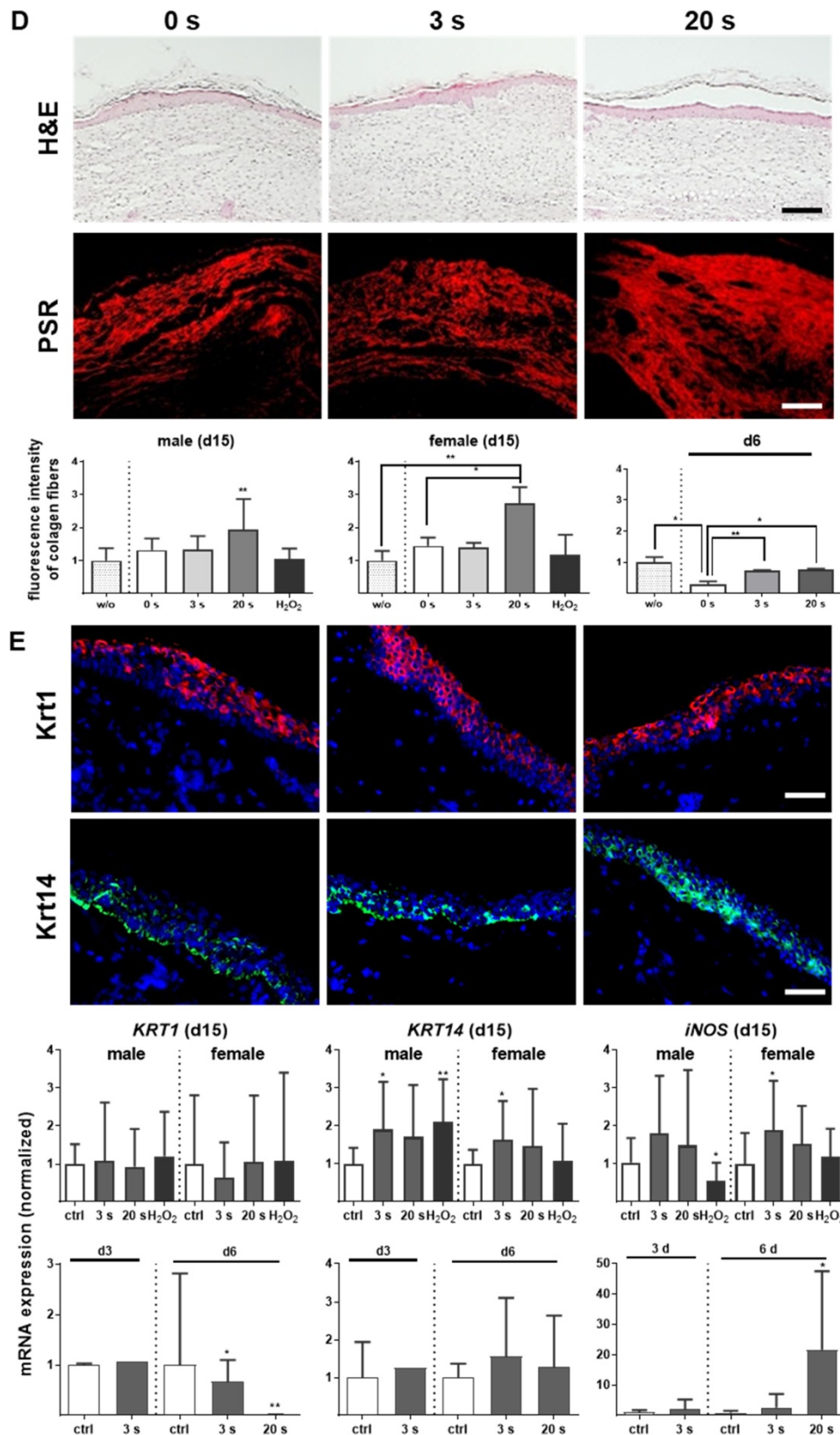


Figure 1. Plasma treatment significantly accelerated wound healing in both male and female mice. (A-B) Representative images of wound healing progress in the treatment (treatment time as indicated) and control groups on days 0 (I), 6 (I¹) and 9 (I^{1*}). White circles represent wound margins in males (A) and females (B). (C) Wound closure was monitored by transmitted light stereomicroscopy and quantified by ImageJ software on every third day over 15 days and related to wound size on the day of surgery (d0). The wound closure rate is plotted as the percentage reduction of the original wound area over time for males (left) and females (right) when compared to the untreated controls. (D-E) Hematoxylin and eosin (H&E), picrosirius red (PSR), keratin 1 (KRT1, red), and keratin 14 (KRT14, green) staining of ear wounds on day 15. Quantification of collagen fibers using fluorescence microscopy (diagrams in D) and qPCR of *KRT1*, *KRT14*, and inducible nitric oxide synthase (*iNOS*) on all time points (diagrams in E). Males and females were used on d15 (as indicated, n > 8); on d3/d6 only females were available for the measurements (n > 3). Data are presented as mean ± S.D.; *p<0.05, **p<0.01, as compared to controls (ctrl / 0 s) at each day and assay; scale bars are 1 mm (A) and 50 µm (D-E).

Table 2: Plasma-induced effects on wound healing evaluated on days 6 and 15 using parameters to qualitatively assess healing scores with regard to collagen pattern (distribution, fiber orientation, early and mature collagen, amount of collagen), inflammation (inflammatory infiltrate), granulation (granulation tissue, cell accumulation, cell migration), angiogenesis (blood vessel formation, vascularization), and apoptosis (blebbing, shrinking, condensation); n.d. = not determined, * $p < 0.05$; ** $p < 0.01$; *** $p < 0.001$) modified from [12, 54, 81]. Each feature was graded from 1 (worst) to 5 (best) regarding healing.

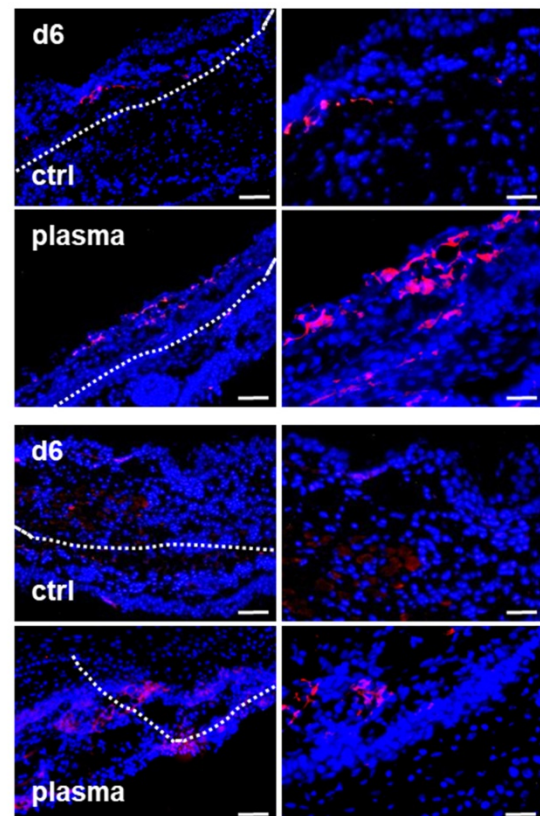
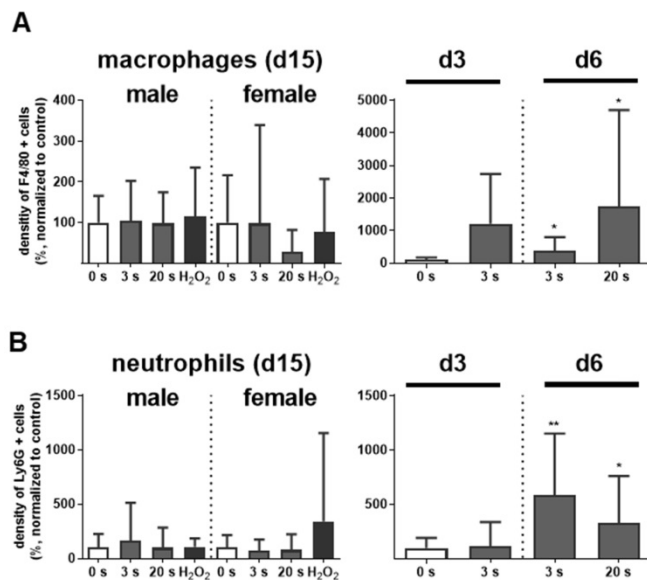
Features	Time point	ctrl	3 s	20 s	H ₂ O ₂
Collagen pattern	d6	2.0 ± 0.1	2.5 ± 0.1**	2.5 ± 0.1*	n.d.
	d15	3.0 ± 0.2	3.3 ± 0.2	3.9 ± 0.4**	3.1 ± 0.2
Inflammation	d6	1.0 ± 0.2	4.8 ± 1.3*	4.4 ± 2*	n.d.
	d15	1.0 ± 0.3	1.4 ± 0.6	2.2 ± 1.3	1.5 ± 0.6
Granulation	d6	1.0 ± 0.06	2.5 ± 0.01**	2.5 ± 0.02*	n.d.
	d15	1.1 ± 0.2	1.0 ± 0.09	1.5 ± 0.25*	1.1 ± 0.17
Angiogenesis	d6	n.d.	n.d.	n.d.	n.d.
	d15	2.1 ± 0.9	3.4 ± 1.2*	3.1 ± 0.7*	2.4 ± 0.8
Apoptosis	d6	1.0 ± 0.18	2.9 ± 0.20***	2.7 ± 0.16***	n.d.
	d15	1.0 ± 0.09	1.4 ± 0.08*	1.1 ± 0.09	1.0 ± 0.17
Mean score	d15	1.47 ± 0.25	2.56 ± 0.42	2.65 ± 0.56	1.82 ± 0.39

No alterations in the early keratinocyte differentiation marker keratin 1 (*KRT1*) were observed, either with immune fluorescence microscopy or qPCR on day 15. Using the same methods, we identified significantly pronounced keratin 14 (*KRT14*) on day 15 in the plasma groups. Additionally, an early and sustained accumulation of

inducible nitric oxide synthase (*iNOS*) was found providing evidence of the anti-microbial properties of cold plasmas (**Figure 1E**).

Plasma-treated wounds showed an inflammatory profile distinct from control wounds

Myeloid cell influx and differentiation dictates the inflammatory response in injury. Significantly more macrophages and neutrophils were found in plasma-treated wounds on day 6 and their presence was confirmed with immune fluorescence (**Figure 2A-B**). On day 3 in females, only a tendency of increase of F4/80 and Ly6G-density was demonstrated. This effect was finished on day 15. Scattered inflammatory cell aggregation or multinucleated swollen macrophages were not detected in H&E or immune fluorescence staining (**Figure 1D**). To map the temporal inflammatory expression pattern, we performed expression and secretion analyses of several cytokines at different intervals during wound healing. The induction of interleukin 1 β (*IL-1 β*), *IL-6*, and tumor-necrosis factor α (*TNF α*) were particularly rapid and strong. In contrast to this proinflammatory profile, *MCP-1* and *IL-4* were in tendency reduced on days 3 and 6 in the plasma groups.



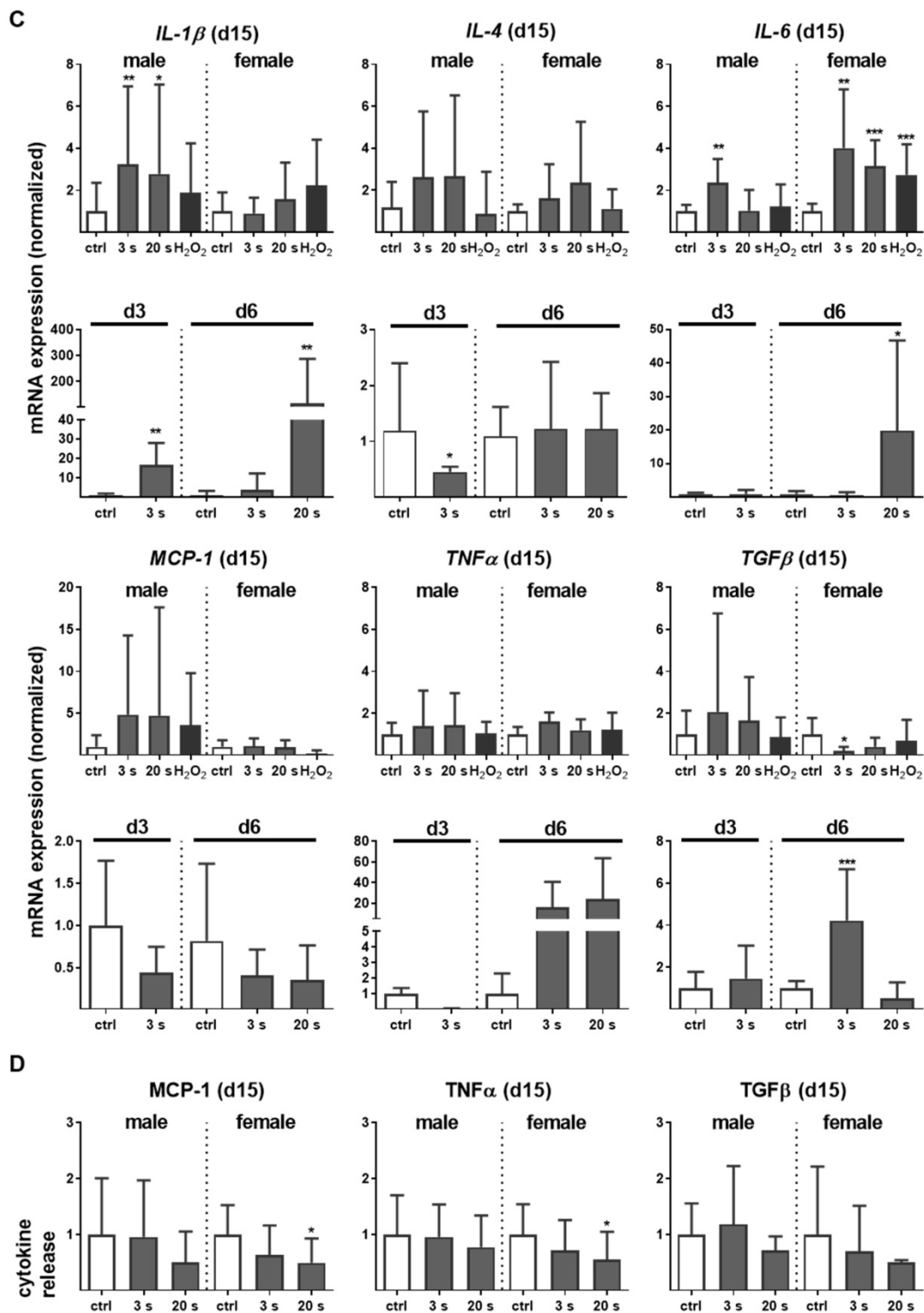


Figure 2. Plasma-treated wounds show a modulated cytokine pattern with increased early myeloid cell infiltrate. (A-B) Density (in %, normalized to controls which were set to 100) and distribution of F4/80-positive macrophages (A) and Ly6G-positive neutrophils (B) in the skin after 3, 6, and 15 days. Representative images of F4/80- and Ly6G-stained (red) cells in wound regions (above the dashed line) on day 6 in plasma-treated compared to untreated mice. Scale bars are 50 μm (left images) or 20 μm (right images; higher magnification). **(C)** mRNA gene expression of inflammatory mediators *IL-1β*, *IL-4*, *IL-6*, *MCP-1*, *TNFα*, and *TGFβ*. **(D)** Cytokine secretion into the blood was measured for MCP-1, *TNFα*, and *TGFβ* 15 days after wounding using multiplex cytokine analysis. Males and females were used on d15 (as indicated; n ≥ 8); on d3/d6 only females were available for the measurements (n > 3). Data are presented as mean ± S.D.; *p<0.05, **p<0.01, ***p<0.001, as compared to controls (ctrl) at each day and assay.

Moreover, the transforming growth factor β (*TGFβ*) transcription was elevated on day 6, suggesting an inflammatory counterbalance to transition from the inflammatory to the

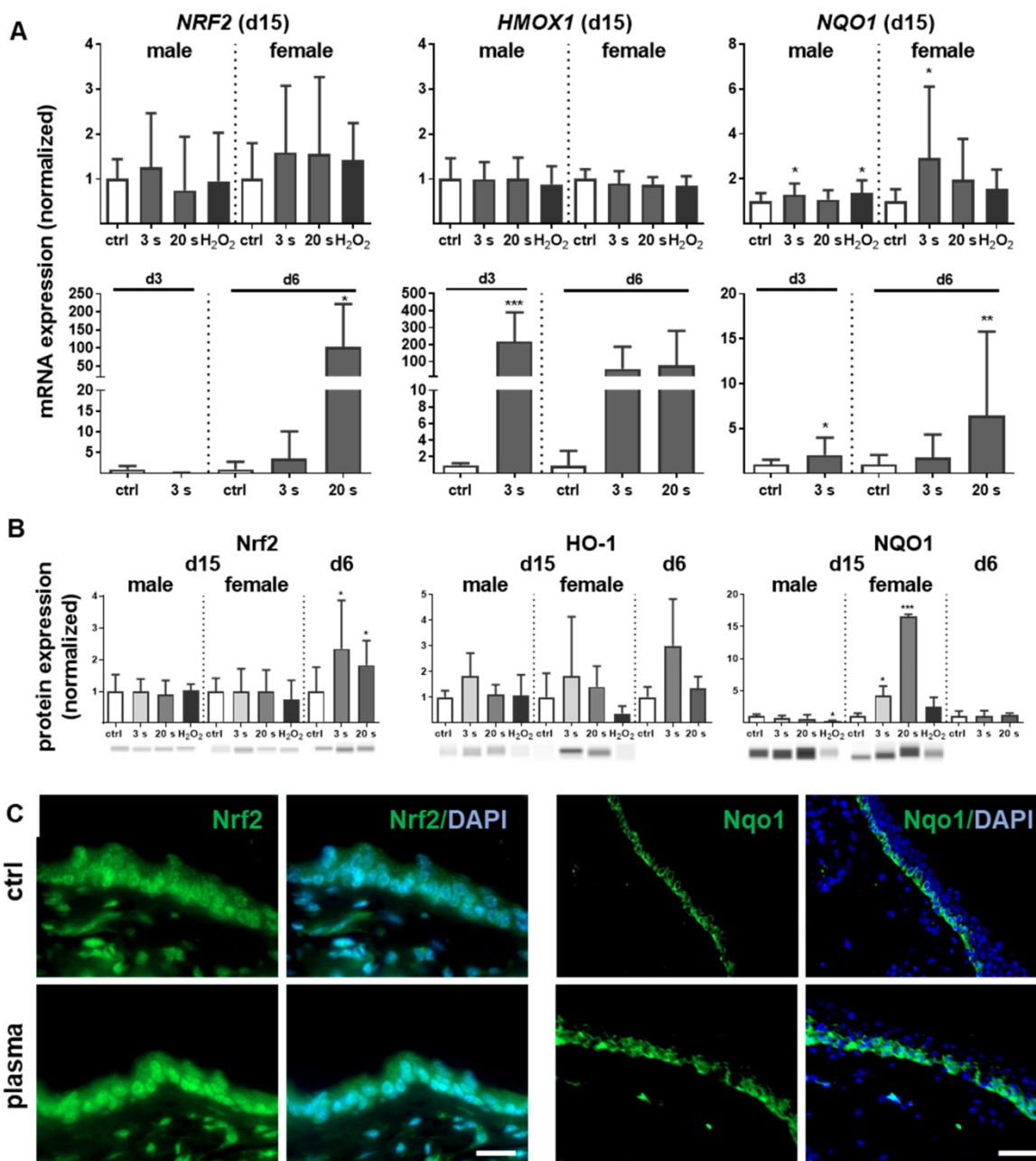
re-epithelization phase (Figure 2C). In females on day 15, a slight downregulation of *TGFβ* was observed, indicating an overshooting anti-inflammatory reaction that may have been responsible for excessive

collagen deposits. Moreover, no significant release of IL-1 β , IL-6 (data not shown), MCP-1, TNF α , and TGF β into the blood serum was observed on day 15 (**Figure 2D**), suggesting the repeated, plasma-induced inflammatory response is non-persistent at a systemic level.

Plasma-treated wounds presented a pronounced Nrf2 signaling signature

Inflammation and antioxidant defense are intimately connected. We identified an upregulation of the master regulator of antioxidant defense (Nrf2) of up to 200 times (**Figure 3A**). A concomitant substantial increase of heme oxygenase 1 (*HMOX1*, gene product of HO-1) levels was detected on day 3

(~250 fold) and day 6 (~100 fold) along with an early (days 3 and 6) and sustained (day 15) activation of NAD(P)H quinone oxidoreductase 1 (*NQO1*) at all time points. Western blot analysis confirmed an increase of Nrf2 at day 6 as well as of HO-1 and Nqo1 in plasma-treated wounds (**Figure 3B**). After plasma treatment and release of Nrf2 from Keap1 by oxidation events at cysteine, Nrf2 translocated to the nucleus as shown in skin sections (left panel in **Figure 3C**). In contrast to the even distribution of Nrf2 within dermal and epidermal layers of the ear skin, Nqo-1 was mainly expressed in the basal epidermal layer as shown by immune fluorescence microscopy (right panel in **Figure 3C**).



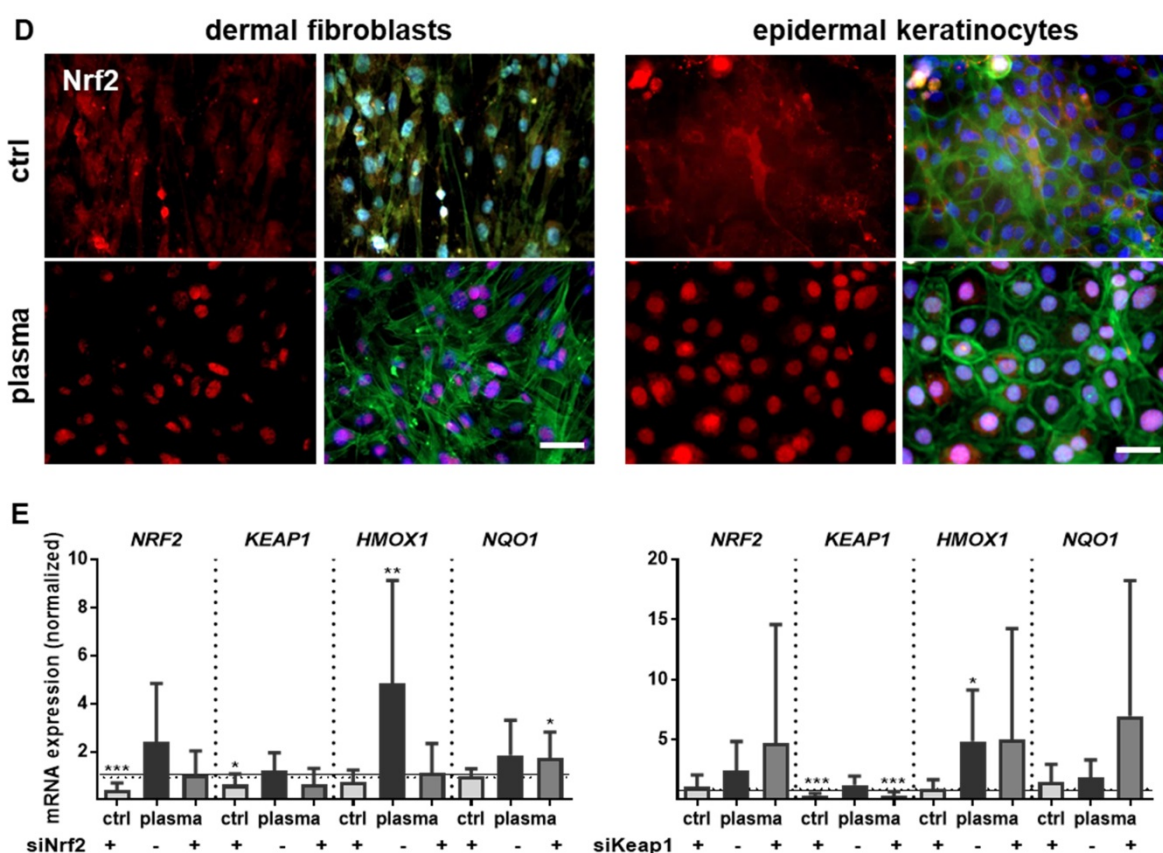


Figure 3. Cold plasma induces an early activation of Nrf2 signaling pathway which controls cellular defense. (A) Mice were treated with cold plasma as described. Quantitative PCR (qPCR) for *NRF2*, *HMOX1* and *NQO1* were performed with total RNAs isolated from the wound regions. (B) Protein expression of Nrf2, HO-1 and Nqo1 was determined using Western blot analysis. (C) Nuclear expression and distribution of Nrf2 (left panel) was shown after plasma treatment by immunofluorescence staining in dermal layers of skin sections. Nqo1 was mainly expressed in the epidermal layer of the skin (right panel). (D) Nrf2 translocation from cytoplasm (upper images) to the nucleus (lower images) after plasma treatment (60 s) was shown in dermal fibroblasts (left) and in epidermal keratinocytes (right). (E) Changes in mRNA expression following siRNA-mediated transcriptional repression of *NRF2* (left diagram) and *KEAP1* (right diagram) in keratinocytes evaluated for *NRF2*, *KEAP1*, *HMOX1*, and *NQO1* by qPCR. The mRNA level of scrambled siRNA were set to 1.14 and 0.91 (black lines) whereas the mRNA and protein levels of untreated mice or mock control without siRNA were set to 1 (dashed line) with $n = 3$ to 9 mice depending on time point. Males and females were used on d15 (as indicated); on d3/d6 only females were available for the measurements. Data are presented as mean \pm S.D.; * $p < 0.05$, ** $p < 0.01$, *** $p < 0.001$, as compared to controls (ctrl) at each day and assay.

Moreover, nuclear translocation of Nrf2 was demonstrated *ex vivo* in dermal fibroblasts and epidermal keratinocytes (Figure 3D) underlining the plasma-mediated activation of the Nrf2 pathway. To identify Nrf2-regulated genes following plasma treatment, Nrf2 and Keap1 were knocked down in keratinocytes (Figure S2). Basal expression of *NRF2*, *KEAP1*, and *HMOX1* was decreased after Nrf2 inhibition, which could not be rescued by plasma treatment (Figure 3E). Conversely, blockage of the physiological Nrf2 inhibitor through siRNA targeting Keap1 resulted in normal baseline levels of *HMOX1*, *NRF2*, and *NQO1*, with plasma treatment not, or only moderately, increasing them. Results (Figure 3D and 3E) are from primary cells of male mice, and were similar for those of female mice (data not shown).

Nrf2 regulates antioxidative response (ARE) genes. Expectedly, plasma treatment not only enhanced Nrf2 expression but also that of downstream targets, such as catalase (*CAT*),

thioredoxin (*TRX*), glutathione reductase (*GSR*), and glutathione peroxidase 2 (*GPX2*). In contrast, cytoplasmic superoxide dismutase (*SOD1*) was significantly decreased by twofold changes on days 3 and 6 (Figure 4A). Western blot analysis confirmed a translational regulation of peroxiredoxin 6 (*Prdx6*), *Sod1*, *Cat*, thioredoxin reductase 1 (*Trxr1*), and *GSR* that was orchestrated by plasma treatment (Figure 4B). Next, down-stream targets of Nrf2 were analyzed in Nrf2 knockdowns, which resulted in the expected reduction of downstream target baseline levels (control columns for each target). In contrast to *GSR*, *GCLC*, and *GCLM*, mRNA was significantly increased after plasma treatment of knockdowns in primary cells of male mice (Figure 4C), with similar findings made with female mice (data not shown). This indicates an inverse regulation of both subunits. In summary, Nrf2 is a key response pathway to plasma treatment in skin cells *in vitro* and in skin *in vivo*.

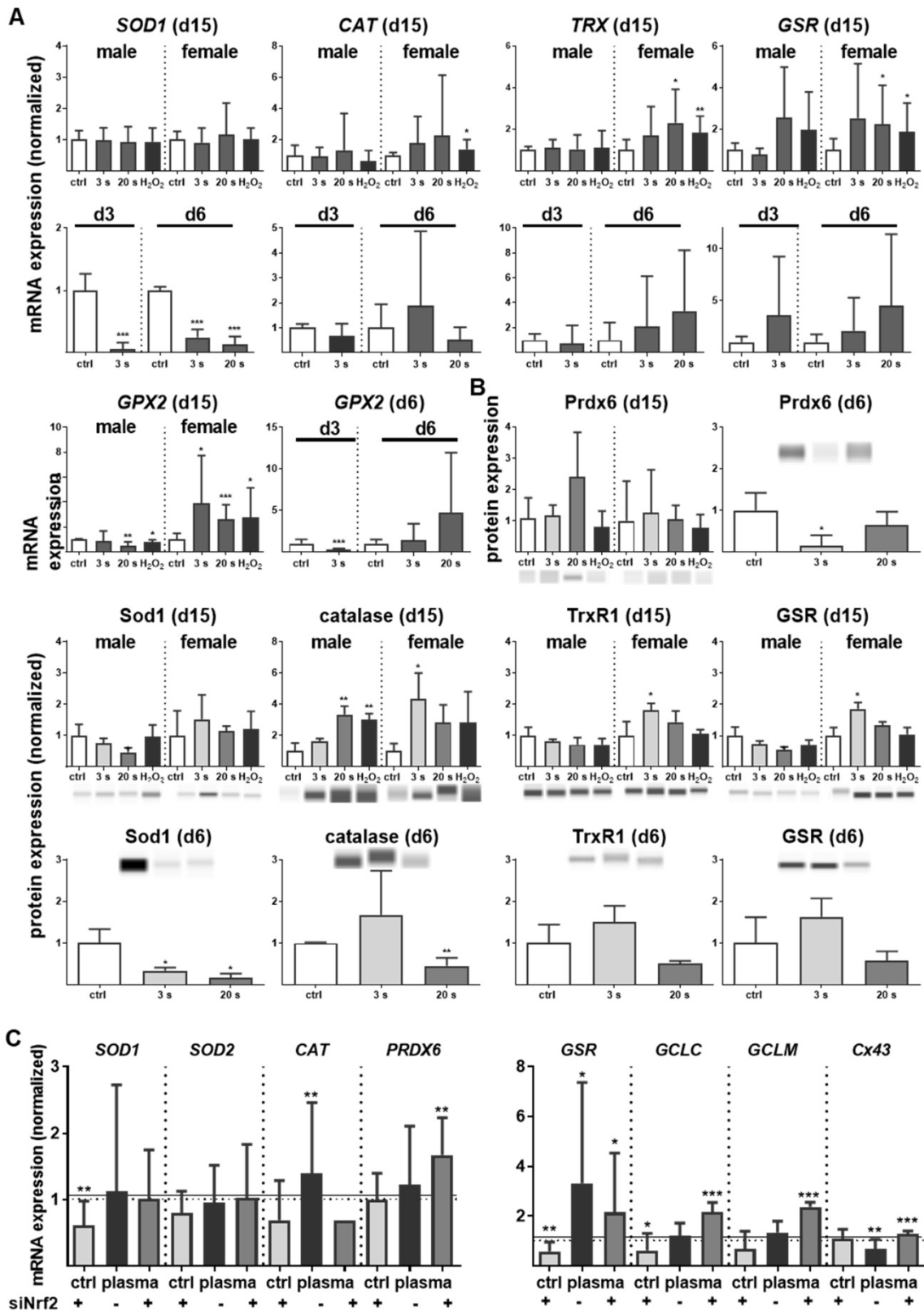


Figure 4. Cold plasma increased antioxidants in skin tissues and cells. (A) The mRNA expression levels in ear skin tissues from plasma-treated and untreated (ctrl) mice were compared and summarized in the indicated experimental groups: *SOD1*, superoxide dismutase 1; *CAT*, catalase; *TRX*, thioredoxin; *GSR*, glutathione reductase; *GPX2*, glutathione peroxidase 2. (B) Western blot analysis of peroxidoreductase 6 (PRDX6), Sod1, catalase, thioredoxin reductase 1 (TRXR1), and GSR. (C) Keratinocytes were transfected with siRNA targeting *NRF2* and evaluated for *SOD1*, *SOD1*, *CAT*, *PRDX6*, *GSR*, *GCLC*, *GCLM*, and *Cx43* mRNA expression by qPCR. The mRNA level of scrambled siRNA and mocked control without siRNA were set to 1.14 (black lines) and 1 (dashed lines), respectively. The mRNA and protein level of untreated mice were arbitrarily set to 1 with n = 3 to 9 mice depending on time point (dashed lines in d and g). Males and females were used on d15 (as indicated); on d3/d6 only females were available for the measurements (n ≥ 3). The data are presented as mean ± S.D.; *p < 0.05, **p < 0.01, ***p < 0.001, as compared to controls (ctrl) at each day and assay.

Plasma-treated wounds were enriched for angiogenic factors and microvessels

Antioxidant defense and inflammation are necessary factors in wound healing but are insufficient without adequate blood supply. Therefore, neovascularization and growth factor expression were studied in control and plasma-treated ear wounds. Throughout all sampling time points, plasma therapy significantly upregulated *CD31* (Figure 5A). Similarly, keratinocyte (*KGF*), basic fibroblast (*bFGF*), vascular endothelial (*VEGFA*), heparin-binding EGF-like (*HBEGF*), and colony stimulating (*CSF2*) growth factors were increased (Figure S2D), suggesting an improved wound vascularization. Inducible cyclooxygenase *COX2* is fundamentally crucial in angiogenesis [33] and was strongly induced during the late stages of wound healing in plasma-treated mice. Furthermore, a moderate down-regulation of VE-cadherin (*CDH5*) on day 15 was observed (Figure 5A). Immune histochemical staining of wound tissue sections confirmed corresponding changes of the major angiogenic factors such as *CD31* and *KGF* (Figure 5B). Using Western blot analysis, we showed a moderate increase of *KGF* protein whereas the serine/threonine kinase *Akt* and the phosphorylated form of *Akt* (*p-Akt*) were significantly increased, especially in females (Figure 5C). Both are known to control several events that are critical for angiogenesis and homeostasis [34]. Significant changes in mRNA expression levels of others angiogenic mediators such as endothelial *NOS* (*eNOS*), artemin 1 (*ARTN1*), endothelin 1 (*EDN1*), ephrin 2 (*EFNB2*), platelet-derived growth factor receptor *CD140a*, matrixmetalloproteinase (*MMP9*), or inhibitor of *MMP* (*TIMP1*) during plasma-promoted wound healing were not detected (data not shown).

To monitor microvessel networks directly, intravital microscopy was performed and revealed newly formed microvessel in a radial and circular pattern (Figure 6A-B). At day 6, the diameter and density of radial and circular vessels did not significantly differ between groups and were therefore not presented in detail. The resolution of microvessel pattern shown by intravital microscopy was limited due to the technical errors in FITC-dextran injections and hence not quantified. Scoring of neovascularization is described in Table 2. On day 15, the microvessel network (Figure 6C) was additionally quantified by determination of vessel diameters and functional microvessel density (FMD). No significant difference for radial or circular diameters was observed effect with 3 s or 20 s plasma treatment (from 5.9 ± 0.4 μm to 6.9 ± 0.4 μm) when compared to controls (from 5.8 ± 0.3 μm to 6.4 ± 0.3 μm)

(Figure 6D). Although, the FMD was between 220 and 230 cm/cm^2 in surrounding tissue (data not shown), the FMD was relatively low (mean level 130 cm/cm^2) in the wound area in all experimental groups. However, and compared to controls (appr. 120 cm/cm^2), FMD significantly increased upon plasma treatment (135 to 150 cm/cm^2 , Figure 6E) but did not reach the same level as in the surrounding tissue at this time point. Nevertheless, the findings support the notion of enhanced angiogenesis in plasma-induced healing.

Plasma-treated wounds promoted dermal proliferation while showing fewer apoptosis

Proliferation and apoptosis are prerequisites to wound healing. Plasma treatment significantly increased basal proliferation on days 3 and 6 (day 15 in tendency), as seen with Ki67-positive cells in the wound region (Figure 7A). Conversely, apoptotic cells were significantly decreased in the plasma groups on day 6. On day 15, there were only slight differences in the number of apoptotic cells in the wound region (Figure 7B). The lower frequency of TUNEL⁺ apoptotic cells may be due either to enhanced macrophage numbers and activity, or a redox-mediated suppression mediated by plasma-derived reactive species. To test the latter option, transcriptional modulation of p53 and its downstream targets of the apoptotic branch *BBC3/Puma* (a p53 upregulated modulator of apoptosis), the pro-apoptotic *BAX*, the anti-apoptotic *BCL2*, the cell cycle arrest branch with *CDKN1A* (encoding p21), and the DNA repair branch (*GADD45a*) were investigated. Plasma treatment mainly inhibited p53 and *BAX* expression at early wound stages, whereas *PUMA* protein expression was moderately but significantly down-regulated in females on day 15 (Figure 7C-D). In contrast, the anti-apoptotic *Bcl2* was upregulated 50-fold on day 6 in the 20 s plasma group but decreased to baseline levels on day 15 (Figure 7E). *CDKN1A* (Figure 7F), encoding protein p21 (data not shown), and *Gadd45a* expression (Figure 7G) remained largely unchanged at all sampling time points and treatment conditions. This finding suggests negligible toxicity or genotoxic stress as a result of exposure to plasma-derived reactive species. Additionally, qualitative (Figure S1D) and quantitative (qPCR, data not shown) measurements failed to find increased levels or increased phosphorylation of histone A2X, a marker of DNA damage and repair.

Discussion

The idea that wound healing was subject to redox control was proposed more than a decade ago

[35]. Although numerous findings in this regard were made while investigating cell-derived reactive species, the application of short-lived exogenous species triggering the same wound-spurring redox pathways has been limited to date. Cold physical plasma is a technology that generates a multitude of

reactive species in the gas phase that are transported to tissues. Here, we not only demonstrated the capacity of plasma to enhance wound healing, but also provided mechanistic insight on crucial changes in inflammation and signaling pathways that are associated with improved healing responses.

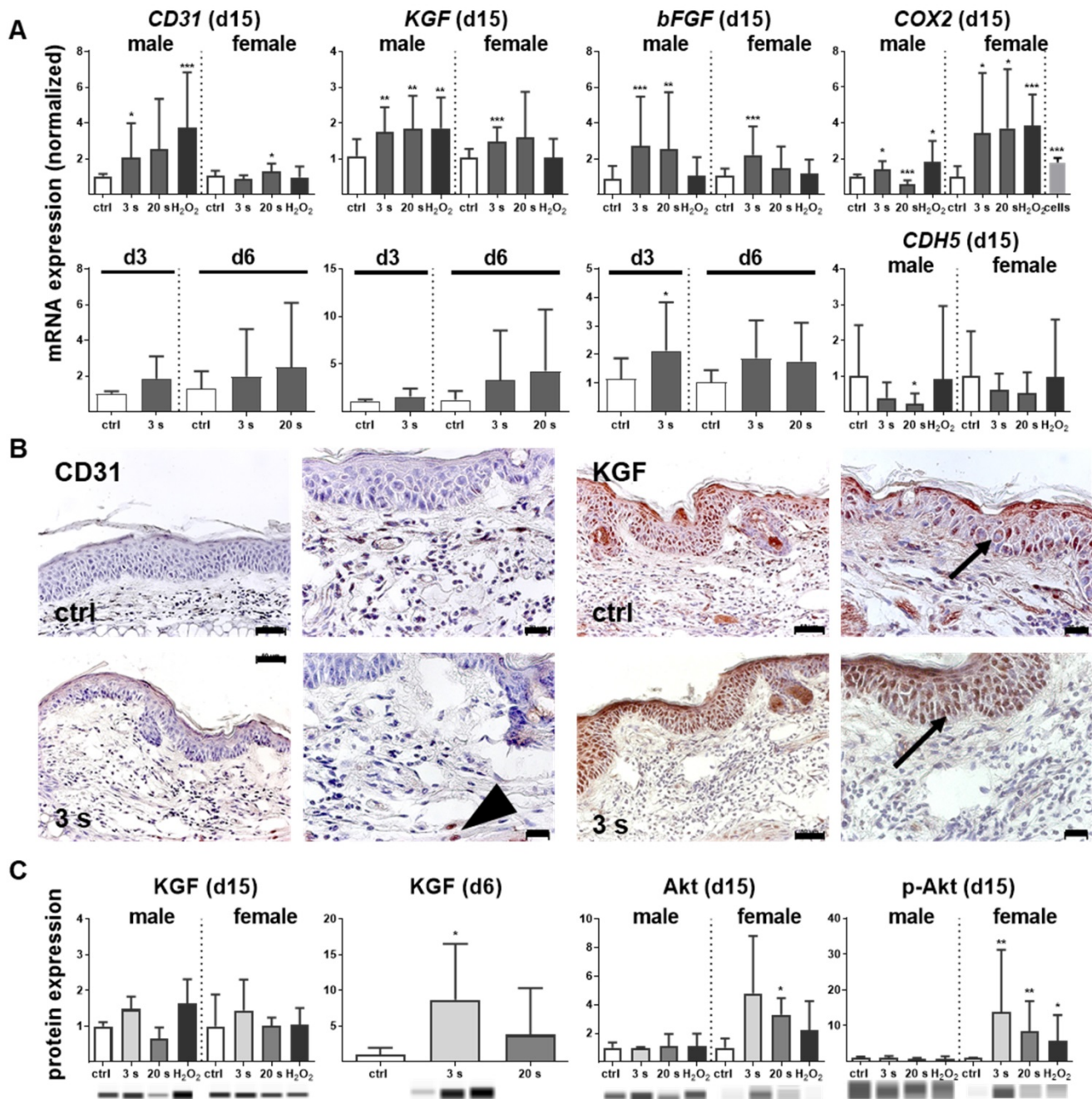


Figure 5. Promotion of pro-angiogenic factors in plasma-treated wounds. (A) SKH1 mice were either exposed to plasma for 3 s or 20 s or were left untreated (ctrl). The mRNA level of *CD31* was strongly increased on day 15 (***p* < 0.01). Both the basic FGF (*bFGF*) and *KGF* (*FGF7*) were significantly upregulated in the plasma-treated animals at all time points. Cyclooxygenase (*COX2*) and VE-cadherin (*CDH5*) were only regulated on day 15 in the plasma-treated groups. (B) Immunohistological staining confirmed a stronger expression of *CD31* (arrowhead) and *KGF* (asterisks) after 6 days in plasma-treated animals compared to controls. Scale bar is 50 μm. (C) *KGF* protein expression showed a significant increase on day 6 whereas *Akt* and phospho-*Akt* proteins were up-regulated in plasma-treated females. Males and females were used on 15 (as indicated, *n* > 8); on d3/d6 only females were available for the measurements (*n* > 3). The data are presented as mean ± S.D.; **p* < 0.05, ***p* < 0.01, ****p* < 0.001, as compared to controls (ctrl) at each day and assay.

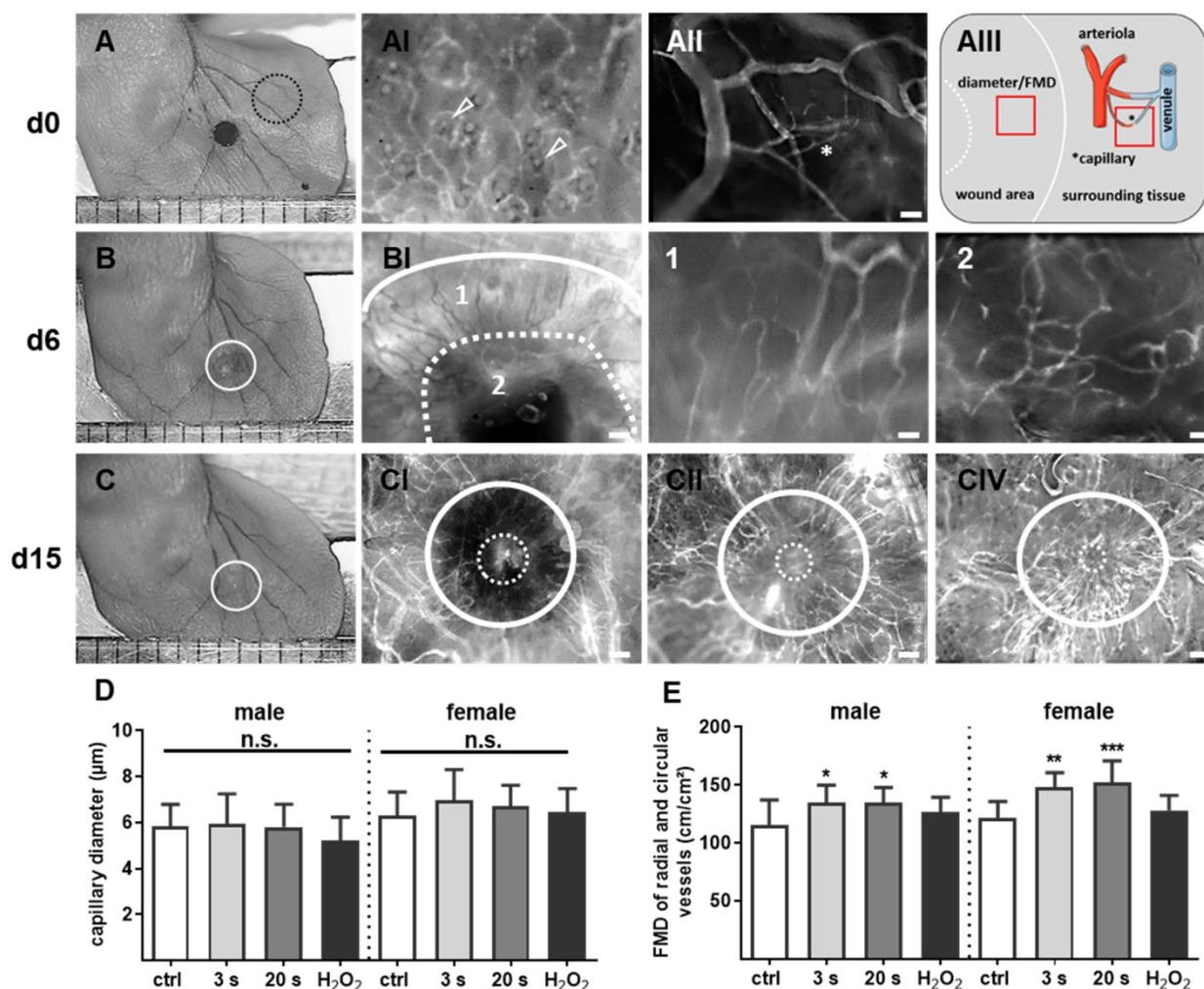


Figure 6. Plasma-supported formation of microvascular network during wound healing. (A-C) Representative photomicroscopic images of ears and intravital fluorescence microscopy images of microvascular features in wound regions (white circles). (A) A typical microvascular architecture of non-wounded skin with papillary loops around empty hair follicles (arrowheads in black dashed circle) is shown in hairless mouse (AI). Visualization of arterioles, venules and capillary (*) in the ear tissue (AII) and schema of diameter and functional microvessel density (FMD) measurements in one cm² (quadrat) in wound area and surrounding tissue (AIII). (B) During the first days of wound healing (d6), the microvessel network creates an outer ring of radial vessels (BI; higher magnification in 1) and an inner circular ring (dashed line) to the wound margin (BI, higher magnification in 2). (C) Novel formed microvessels are between white circles in untreated controls (male, CI), plasma-treated males (CII), and plasma-treated females (CIII). The white continuous line marks wound area on day of wounding, the dashed line represents the eye of wound at indicated time points. Scale bars are 1 mm (A-C); 200 μm (AI-II, BI, CI-III); 50 μm (BI-2). (D-E) Quantitative analysis of vessel diameter (μm) and FMD (cm/cm²) in both gender (n≥3). Males and females were used on d15 (as indicated, n > 8); on d3/d6 only females were available for the measurements. The data are presented as mean ± S.D.; *p<0.05, **p<0.01, ***p<0.001 using one-way ANOVA.

We identified the pivotal involvement of the redox-regulating Nrf2 and p53 signaling pathway in cold plasma-treated wounds. Redox signaling transcriptionally controls protein and enzyme activity as well as post-translational modifications such as nitrosylation, hydroxylation, and glutathionylation [36]. Nrf2, as a gatekeeper of intra- and extra-cellular redox signals, enables responses to oxidizing noxae [37]. Glutathione (GSH) metabolism via transcriptional modulation of *GSR* [38] and the antioxidant glutathione peroxidases (*GPX*) [39] are also under the control of Nrf2. We found a protective Nrf2 signaling in response to plasma that counteracted oxidative stress via upregulation of its down-stream targets such as catalase, peroxiredoxins, and thioredoxins (*TRX*) during wound healing. Through reactive species-induced oxidation of Keap 1

cysteines, which act as redox-sensor, activation of Nrf2 is allowed, leading to an increase in antioxidant defense, which was also shown in human keratinocytes *in vitro* [28], further supporting our findings in this study. *TRX* functions to reduce oxidized target protein cysteine disulfides that were generated from excess oxidants [40]. *CDKN1A*, another target of Nrf2 [41], is a key downstream molecule of p53 modulating cell-cycle and glutathione metabolism that again feeds into antioxidant defense [42].

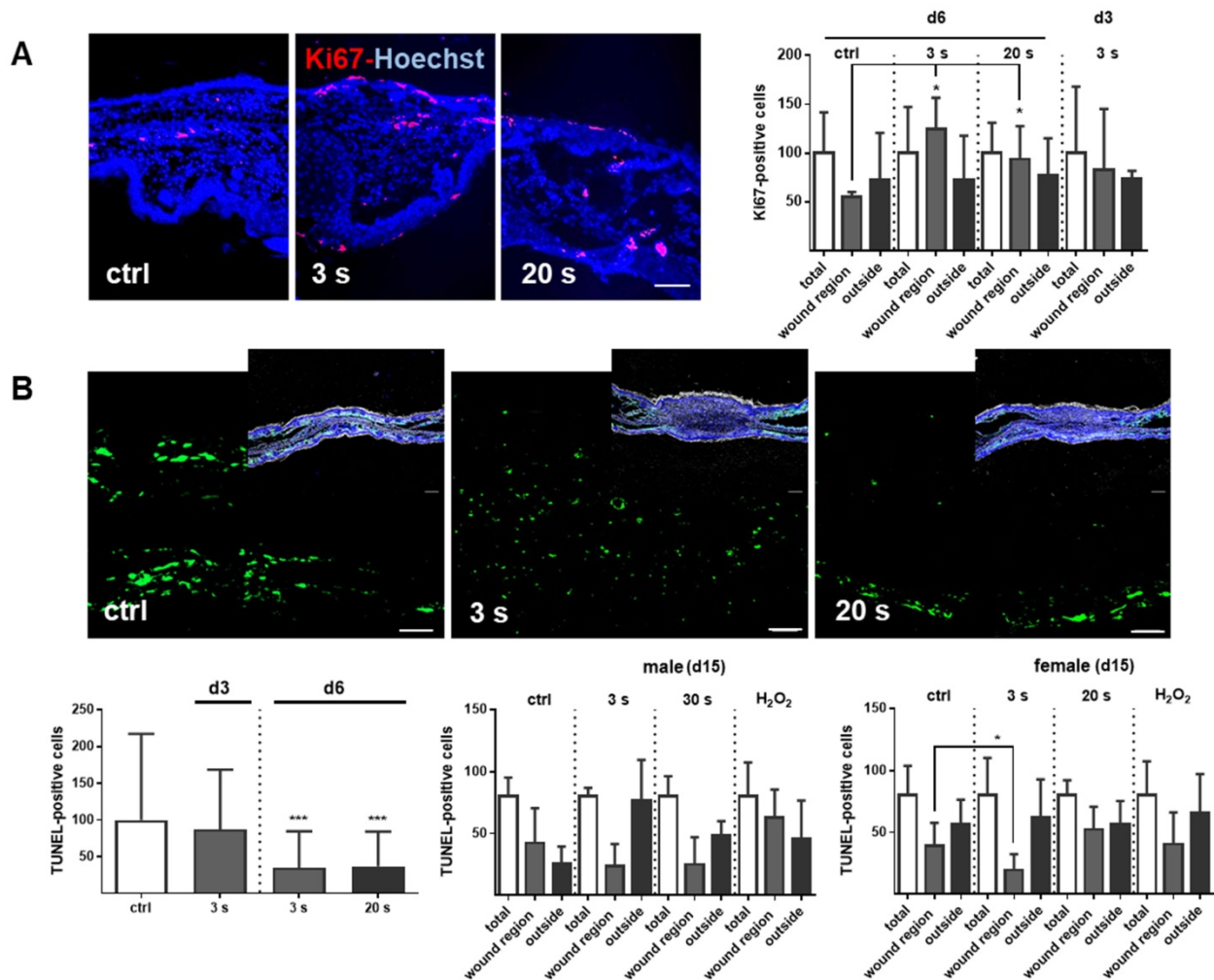
Nrf2 also signals inflammation via inhibition of NF-κB [43], activation of *HMOX1* (encoding HO-1), and *COX2* [44]. A previous study found that Nrf2-ARE-driven genes such as *HMOX1*, *NQO1*, and glutamate cysteine ligase (catalytic *GCLC* and regulatory subunit *GCLM*) block monocyte

chemoattractant protein-1 (MCP-1/CCL2) [43]. Interestingly, we observed a strong up-regulation of *GCLC* and *GCLM* after plasma treatment and Nrf2 knockdown, suggesting that other pathways can compensate the knockdown of Nrf2 *in vitro*. The most likely candidate for this compensatory effect after siRNA targeting Nrf2 is Nrf1/3 [45].

Nrf2 is also a key regulator in macrophages [46]. Macrophages are innate immune cells, which secret and respond to a repertoire of cytokines, e.g. TNF α , in an autocrine or paracrine manner, thus emphasizing the inflammatory response [47]. Their migration, maturation, and phenotyping are tightly controlled throughout physiological wound healing phases [48]. In our study, plasma increased macrophage and neutrophil influx and upregulated pro-inflammatory markers IL-6 or TNF α at early but not later stages of wound healing. This finding suggests that mild inflammation by plasma treatment is necessary to recruit myeloid cells, followed by an increase in

anti-inflammatory and antioxidant pathways such as Nrf2 at early stages. Our *in vitro* results confirmed a Nrf2-dependent inhibiting of pro-inflammatory cytokines as shown by siRNA knockdown targeting Nrf2, which has been demonstrated in previous studies [49].

Cell proliferation and programmed death are dependent on reactive species-mediated signaling [3, 15, 50]. Observational studies of plasma-accelerated reepithelialization and granulation in animals [51-54] and humans [23, 24, 55-57] support this notion. Using Ki67 as a marker, we observed an increase in proliferation and tissue repair and the earlier development and accumulation of granulation tissue, together with increased collagen expression after plasma treatment. p53 and its down-stream targets mediates programmed cell death in wounds [12, 58]. Its activity depends on the stage of wound healing, which our data confirm.



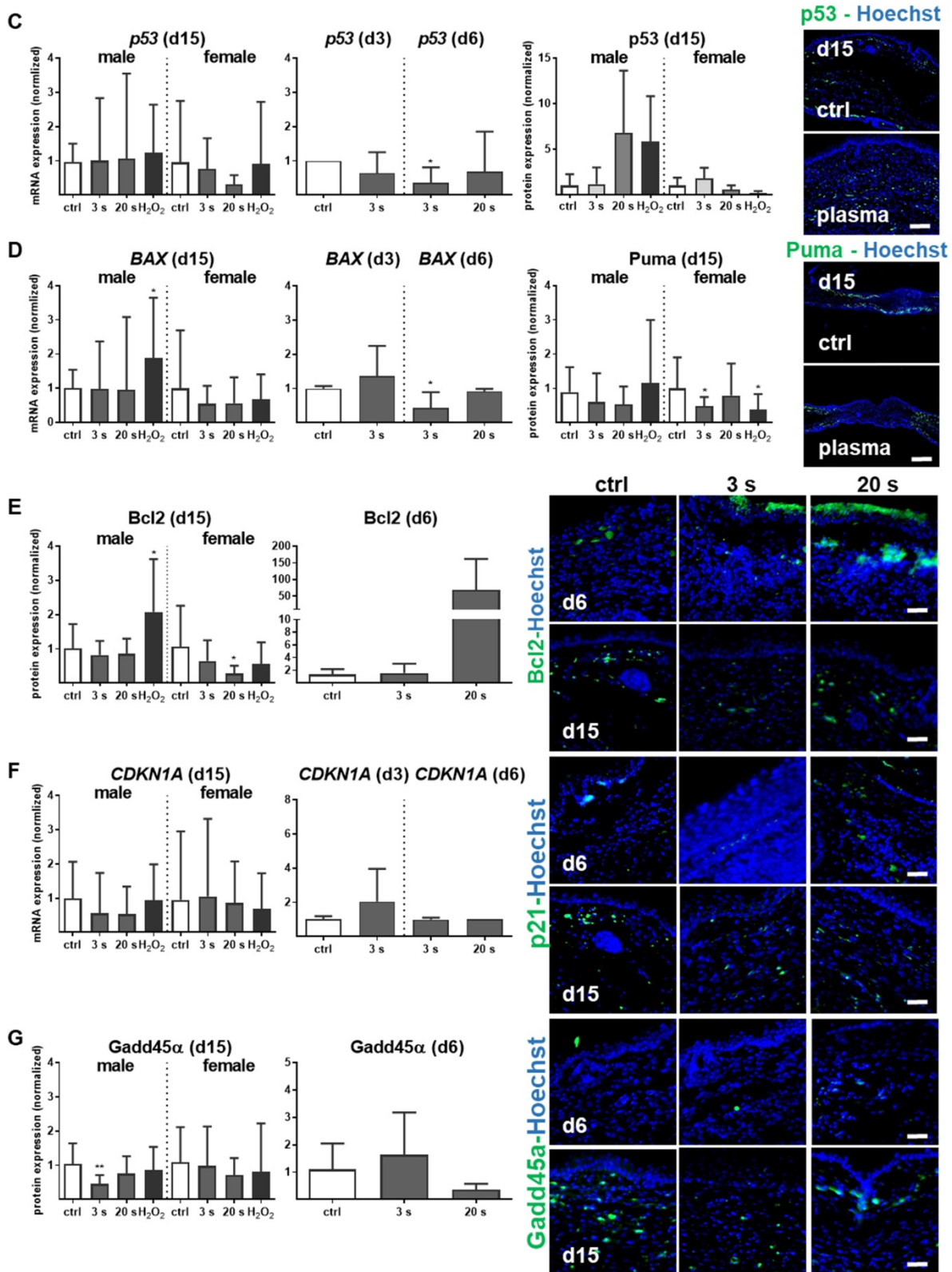


Figure 7. Cold plasma increases proliferation and attenuates tissue apoptosis by regulation of p53 signaling in dependence of wound healing stages. (A) SKH1 mice were either exposed to plasma treatment (3 s and 20 s) or were left untreated (ctrl). Ki67-positive cells (red) were significantly increased in the plasma-treated skin in contrast to untreated mice. (B) TUNEL-positive cells (green) were rarely seen in the dermis of plasma-treated skin (3 s or 20 s) in contrast to untreated mice (ctrl). The nuclei are labeled with Hoechst 33342 (blue). Scale bar is 50 μ m. (A-B) Quantification of Ki67- and TUNEL-positive cells show a significant increase of proliferative cells on day 6 (A) and a decrease of apoptotic cells in the regenerating skin after plasma treatment. Outside of the wound regions, no differences were detected (B). (C-D) Gene expression levels of *p53* and *BAX* (left diagrams) were significantly down-regulated on day 6. *p53* was moderately up-regulated on day 15, which was confirmed by protein expression on day 15 (right diagram). *Puma* protein levels were significantly decreased in females on day 15 (right diagram). (E) The anti-apoptotic protein *Bcl-2* was mainly up-regulated after 6 days but mainly unchanged on day 15. (F-G) *CDKN1A* expression level (F) and *Gadd45a* protein expression (G) were unchanged upon plasma treatment. Males and females were used on d15 (as indicated, n > 8) on d3/d6 only females were available for the measurements (n > 3). The data are presented as mean \pm S.D.; *p < 0.05, **p < 0.01, ***p < 0.001, as compared to controls (ctrl) at each day and assay.

Pro- and anti-apoptotic factors control the removal of inflammatory cells and angiogenesis [59]. Moreover, p53 is central in angiogenesis and essential in the regulation of nitric oxide synthase (NOS) [33]. Our results are consistent with other studies [60] showing that the overexpression of NOS causes the down-regulation of superoxide dismutase 1 (SOD1) [61]. Plasma-released NO [62-64] may be a driver for the increased *iNOS* and *COX2* expression observed here in plasma-treated ear wounds. *COX2* regulates angiogenesis via growth factor expression [65]. Plasma induces the upregulation of growth factor and angiogenic transcripts in human keratinocytes [17], a finding confirmed by this study (e.g. *KGF*, *FGF*, *VEGFA*, *HBEGF*, *CSF2*, *bFGF*, *CD31*, *Akt/p-Akt*). In support of our findings, p53 silencing improved diabetic wounds through augmented CD31 and VEGF expression [66] and KGF receptor activation, which is central during wound healing [34]. Moreover, Akt takes a center stage in angiogenesis signaling [67].

Intravital microscopy (IVM) confirmed that plasma treatment triggered an “angiogenic switch” also known to be induced in principle by other signals such as metabolic and mechanical stress as well as immune and inflammatory responses [68]. The increase of functional microvessel density (FMD) upon plasma treatment may have increased oxygen and nutrient supply into the wounded area. Oxygenation has been suggested to be beneficial in healing of chronic wounds [15]. Interestingly, several studies pointed out the pivotal role of Nrf2 in angiogenesis [69, 70] by promoting vascular development [71], preventing downregulation of insulin and MAPK signaling [72] and reduction of oxidative stress in endothelial cells [73]. Moreover, plasma-induced regulation of Nrf2 and down-stream targets coincided with angiogenesis [74, 75]. Vice versa, Nrf2 dysfunction is responsible for impaired angiogenesis and microvascular rarefaction [76]. In our study, we found knockdown of Nrf2 correlating with a reduced growth factor expression in keratinocytes (**Figure S2**), supporting the view of an accelerated healing response including neovascularization and angiogenesis following plasma treatment.

Our study has limitations. First, we were not able to fully explore the gender dimension of the molecular mechanisms on wound healing on day 6 to possibly explain different healing responses with plasma seen in male vs. female mice. These differences may be explained by mutual cross-talk between redox and hormone signaling [77], as demonstrated before [78-80]. Second, defective wound healing in patients often is a problem of the elderly. Our study design intended to address the

molecular mechanisms of plasma-induced wound healing, and understanding the role of age in these processes may be a subject of future studies.

In summary, repetitive treatment with cold physical plasma-derived reactive species promoted early ear wound closure in SKH1 mice. This finding was associated with an enhanced infiltration of macrophages and neutrophils, an upregulated transcription of both pro-inflammatory and anti-inflammatory mediators, increased proliferation and decreased apoptosis, a spurred antioxidative defense response driven by Nrf2, and enhanced angiogenesis. Wound healing is a multifactorial process. Hence, isolating a single above mentioned effector as the main driver of reactive species-driven acceleration in wound healing would be inappropriate. Instead, redox-driven processes that are initiated with plasma-derived species appear capable of spurring several physiological processes. Unraveling their molecular details may support new avenues for skin regeneration and, importantly, for treating poorly healing wounds.

Abbreviations

ARE: antioxidant response element; Keap1: Kelch-like ECH-associated protein 1; Nrf2: nuclear factor-erythroid 2-related factor 2; RNS: reactive nitrogen species; ROS: reactive oxygen species.

Supplementary Material

Supplementary figures and tables.

<http://www.thno.org/v09p1066s1.pdf>

Acknowledgments

The authors thank Liane Kantz, Caner Özer, Uyen My Vu (all INP Greifswald, Germany), and Dorothea Frenz (IEC, University of Rostock, Germany) for their technical support. This work was funded by the Ministry of Education, Science, and Culture of the State of Mecklenburg-Western Pomerania (Germany), the European Union, European Social Fund (grant numbers AU 11 038; ESF/IV-BM-B35-0010/13 and AU 15 001), and the German Federal Ministry of Education and Research (grant number 03Z22DN11).

Author contributions

All authors contributed to this study: AS designed and performed the experiments. BV provided the mouse model. All authors wrote the manuscript.

Competing Interests

The authors have declared that no competing interest exists.

References

- Broughton G, 2nd, Janis JE, Attinger CE. The basic science of wound healing. *Plast Reconstr Surg*. 2006; 117: 12S-34S.
- Sies H. Oxidative stress: a concept in redox biology and medicine. *Redox Biol*. 2015; 4: 180-3.
- Roy S, Khanna S, Nallu K, Hunt TK, Sen CK. Dermal wound healing is subject to redox control. *Mol Ther*. 2006; 13: 211-20.
- Sen CK, Gordillo GM, Roy S, Kirsner R, Lambert L, Hunt TK, et al. Human skin wounds: a major and snowballing threat to public health and the economy. *Wound Repair Regen*. 2009; 17: 763-71.
- Jazayeri L, Callaghan MJ, Grogan RH, Hamou CD, Thanik V, Ingraham CR, et al. Diabetes increases p53-mediated apoptosis following ischemia. *Plast Reconstr Surg*. 2008; 121: 1135-43.
- Botusan IR, Sunkari VG, Savu O, Catrina AI, Grunler J, Lindberg S, et al. Stabilization of HIF-1alpha is critical to improve wound healing in diabetic mice. *Proc Natl Acad Sci U S A*. 2008; 105: 19426-31.
- Callaghan MJ, Ceradini DJ, Gurtner GC. Hyperglycemia-induced reactive oxygen species and impaired endothelial progenitor cell function. *Antioxid Redox Signal*. 2005; 7: 1476-82.
- Wetzler C, Kamper H, Stallmeyer B, Pfeilschifter J, Frank S. Large and sustained induction of chemokines during impaired wound healing in the genetically diabetic mouse: prolonged persistence of neutrophils and macrophages during the late phase of repair. *J Invest Dermatol*. 2000; 115: 245-53.
- Nguyen KT, Seth AK, Hong SJ, Geringer MR, Xie P, Leung KP, et al. Deficient cytokine expression and neutrophil oxidative burst contribute to impaired cutaneous wound healing in diabetic, biofilm-containing chronic wounds. *Wound Repair Regen*. 2013; 21: 833-41.
- Olovnikov IA, Kravchenko JE, Chumakov PM. Homeostatic functions of the p53 tumor suppressor: regulation of energy metabolism and antioxidant defense. *Semin Cancer Biol*. 2009; 19: 32-41.
- Hanschmann EM, Godoy JR, Berndt C, Hudemann C, Lillig CH. Thioredoxins, glutaredoxins, and peroxiredoxins—molecular mechanisms and health significance: from cofactors to antioxidants to redox signaling. *Antioxid Redox Signal*. 2013; 19: 1539-605.
- Vollmar B, El-Gibaly AM, Scheuer C, Strik MW, Bruch HP, Menger MD. Acceleration of cutaneous wound healing by transient p53 inhibition. *Lab Invest*. 2002; 82: 1063-71.
- Soeur J, Eilstein J, Lereaux G, Jones C, Marrot L. Skin resistance to oxidative stress induced by resveratrol: from Nrf2 activation to GSH biosynthesis. *Free Radic Biol Med*. 2015; 78: 213-23.
- Bitar M. The GSK-3β/Fyn/Nrf2 pathway in fibroblasts and wounds of type 2 diabetes. *Adipocyte*. 2012; 1: 161-3.
- Gristina R, D'Alaia E, Senesi GS, Milella A, Nardulli M, Sardella E, et al. Increasing cell adhesion on plasma deposited fluorocarbon coatings by changing the surface topography. *J Biomed Mater Res B Appl Biomater*. 2009; 88: 139-49.
- von Woedtke T, Reuter S, Masur K, Weltmann KD. Plasmas for medicine. *Phys Rep*. 2013; 530: 291-320.
- Barton A, Wende K, Bundscherer L, Hasse S, Schmidt A, Bekeschus S, et al. Nonthermal Plasma Increases Expression of Wound Healing Related Genes in a Keratinocyte Cell Line. *Plasma Med*. 2013; 3: 125-36.
- Bekeschus S, Schmidt A, Weltmann K-D, von Woedtke T. The plasma jet kINPen – A powerful tool for wound healing. *Clin Plas Med*. 2016; 4: 19-28.
- Arndt S, Landthaler M, Zimmermann JL, Unger P, Wacker E, Shimizu T, et al. Effects of cold atmospheric plasma (CAP) on ss-defensins, inflammatory cytokines, and apoptosis-related molecules in keratinocytes in vitro and in vivo. *PLoS One*. 2015; 10: e0120041.
- Arndt S, Unger P, Wacker E, Shimizu T, Heinlin J, Li YF, et al. Cold atmospheric plasma (CAP) changes gene expression of key molecules of the wound healing machinery and improves wound healing in vitro and in vivo. *PLoS One*. 2013; 8: e79325.
- Kubinova S, Zaviskova K, Uherkova L, Zablotskii V, Churpita O, Lunov O, et al. Non-thermal air plasma promotes the healing of acute skin wounds in rats. *Sci Rep*. 2017; 7: 45183.
- Schmidt A, Bekeschus S, Wende K, Vollmar B, von Woedtke T. A cold plasma jet accelerates wound healing in a murine model of full-thickness skin wounds. *Exp Dermatol*. 2017; 26: 156-62.
- Ulrich C, Kluschke F, Patzelt A, Vandersee S, Czaika VA, Richter H, et al. Clinical use of cold atmospheric pressure argon plasma in chronic leg ulcers: A pilot study. *J Wound Care*. 2015; 24: 198-200, 202-3.
- Brehmer F, Haenssle HA, Daeschlein G, Ahmed R, Pfeiffer S, Gortlitz A, et al. Alleviation of chronic venous leg ulcers with a hand-held dielectric barrier discharge plasma generator (PlasmaDerm(R)) VU-2010): results of a monocentric, two-armed, open, prospective, randomized and controlled trial (NCT01415622). *J Eur Acad Dermatol Venereol*. 2015; 29: 148-55.
- Barker JH, Kjolseth D, Kim M, Frank J, Bondar I, Uhl E, et al. The hairless mouse ear: an in vivo model for studying wound neovascularization. *Wound Repair Regen*. 1994; 2: 138-43.
- Sorg H, Schulz T, Krueger C, Vollmar B. Consequences of surgical stress on the kinetics of skin wound healing: partial hepatectomy delays and functionally alters dermal repair. *Wound Repair Regen*. 2009; 17: 367-77.
- Chen L, Mirza R, Kwon Y, DiPietro LA, Koh TJ. The murine excisional wound model: Contraction revisited. *Wound Repair Regen*. 2015; 23: 874-7.
- Schmidt A, Dietrich S, Steuer A, Weltmann KD, von Woedtke T, Masur K, et al. Non-thermal plasma activates human keratinocytes by stimulation of antioxidant and phase II pathways. *J Biol Chem*. 2015; 290: 6731-50.
- Schmidt A, von Woedtke T, Stenzel J, Lindner T, Polei S, Vollmar B, et al. One Year Follow-Up Risk Assessment in SKH-1 Mice and Wounds Treated with an Argon Plasma Jet. *Int J Mol Sci*. 2017; 18.
- Pang S, Han C, Kato M, Sternberg PW, Yang C. Wide and scalable field-of-view Talbot-grid-based fluorescence microscopy. *Opt Lett*. 2012; 37: 5018-20.
- Sorg H, Krueger C, Schulz T, Menger MD, Schmitz F, Vollmar B. Effects of erythropoietin in skin wound healing are dose related. *FASEB J*. 2009; 23: 3049-58.
- Fahmy SR. Anti-fibrotic effect of *Holothuria arenicola* extract against bile duct ligation in rats. *BMC Complement Altern Med*. 2015; 15: 14.
- Chiarugi V, Magnelli L, Gallo O. Cox-2, iNOS and p53 as play-makers of tumor angiogenesis (review). *Int J Mol Med*. 1998; 2: 715-9.
- Beer HD, Gassmann MG, Munz B, Steiling H, Engelhardt F, Bleuel K, et al. Expression and function of keratinocyte growth factor and activin in skin morphogenesis and cutaneous wound repair. *J Investig Dermatol Symp Proc*. 2000; 5: 34-9.
- Sen CK. The general case for redox control of wound repair. *Wound Repair Regen*. 2003; 11: 431-8.
- Schafer FQ, Buettner GR. Redox environment of the cell as viewed through the redox state of the glutathione disulfide/glutathione couple. *Free Radic Biol Med*. 2001; 30: 1191-212.
- Schafer M, Werner S. Nrf2—A regulator of keratinocyte redox signaling. *Free Radic Biol Med*. 2015; 88: 243-52.
- Harvey SA, Guerriero E, Charukamnoetkanok N, Piluek J, Schuman JS, Sundarraj N. Responses of cultured human keratocytes and myofibroblasts to ethyl pyruvate: a microarray analysis of gene expression. *Invest Ophthalmol Vis Sci*. 2010; 51: 2917-27.
- Lu SC. Regulation of glutathione synthesis. *Mol Aspects Med*. 2009; 30: 42-59.
- Holmgren A. Antioxidant function of thioredoxin and glutaredoxin systems. *Antioxid Redox Signal*. 2000; 2: 811-20.
- Malhotra D, Portales-Casamar E, Singh A, Srivastava S, Arenillas D, Happel C, et al. Global mapping of binding sites for Nrf2 identifies novel targets in cell survival response through ChIP-Seq profiling and network analysis. *Nucleic Acids Res*. 2010; 38: 5718-34.
- Tarangelo A, Magtanong L, Bieging-Rolett KT, Li Y, Ye J, Attardi LD, et al. p53 Suppresses Metabolic Stress-Induced Ferroptosis in Cancer Cells. *Cell Rep*. 2018; 22: 569-75.
- Ahmed SM, Luo L, Namani A, Wang XJ, Tang X. Nrf2 signaling pathway: Pivotal roles in inflammation. *Biochim Biophys Acta*. 2017; 1863: 585-97.
- Itoh K, Mochizuki M, Ishii Y, Ishii T, Shibata T, Kawamoto Y, et al. Transcription factor Nrf2 regulates inflammation by mediating the effect of 15-deoxy-Delta(12,14)-prostaglandin j(2). *Mol Cell Biol*. 2004; 24: 36-45.
- Ohtsuiji M, Katsuoka F, Kobayashi A, Aburatani H, Hayes JD, Yamamoto M. Nrf1 and Nrf2 play distinct roles in activation of antioxidant response element-dependent genes. *J Biol Chem*. 2008; 283: 33554-62.
- Wakabayashi N, Slocum SL, Skoko JJ, Shin S, Kensler TW. When NRF2 talks, who's listening? *Antioxid Redox Signal*. 2010; 13: 1649-63.
- Parameswaran N, Patial S. Tumor Necrosis Factor-α Signaling in Macrophages. *Crit Rev Eukaryot Gene Expr*. 2010; 20: 87-103.
- Short JD, Downs K, Tavakoli S, Asmis R. Protein Thiol Redox Signaling in Monocytes and Macrophages. *Antioxid Redox Signal*. 2016; 25: 816-35.
- Lee DS, Jeong GS. Arylbenzofuran isolated from *Dalbergia odorifera* suppresses lipopolysaccharide-induced mouse BV2 microglial cell activation, which protects mouse hippocampal HT22 cells death from neuroinflammation-mediated toxicity. *Eur J Pharmacol*. 2014; 728: 1-8.
- Sen CK, Roy S. Redox signals in wound healing. *Biochim Biophys Acta*. 2008; 1780: 1348-61.
- Kramer A, Lademann J, Bender C, Sckell A, Hartmann B, Münch S, et al. Suitability of tissue tolerable plasmas (TTP) for the management of chronic wounds. *Clin Plas Med*. 2013; 1: 11-8.
- Falanga V. Wound healing and its impairment in the diabetic foot. *Lancet*. 2005; 366: 1736-43.
- Bender C, Kramer A. Therapy of wound healing disorders in pets with atmospheric pressure plasma. *Tieraerztl Umsch*. 2016; 71: 262-8.
- Fathollah S, Mirpour S, Mansouri P, Dehpour AR, Ghoranneviss M, Rahimi N, et al. Investigation on the effects of the atmospheric pressure plasma on wound healing in diabetic rats. *Sci Rep*. 2016; 6: 19144.
- Metelmann HR, Podmelle F, Waite PD, Muller-Debus CF, Hammes S, Funk W. Conditioning in laser skin resurfacing - betulin emulsion and skin recovery. *J Craniomaxillofac Surg*. 2013; 41: 249-53.
- Metelmann H-R vWT, Bussiahn R, Weltmann K-D, Rieck M, Khalili R, Podmelle F, Waite PD. Experimental recovery of CO2-laser skin lesions by plasma stimulation. *American Journal of Cosmetic Surgery*. 2012; 29: 52-6.
- Emmert S, Brehmer F, Hänßle H, Helmke A, Mertens N, Ahmed R, et al. Atmospheric pressure plasma in dermatology: ulcer treatment and much more. *Clin Plas Med*. 2013; 1: 24-9.
- Antoniades HN, Galanopoulos T, Neville-Golden J, Kiritsy CP, Lynch SE. p53 expression during normal tissue regeneration in response to acute cutaneous injury in swine. *J Clin Invest*. 1994; 93: 2206-14.
- Rai NK, Tripathi K, Sharma D, Shukla VK. Apoptosis: a basic physiologic process in wound healing. *Int J Low Extrem Wounds*. 2005; 4: 138-44.

60. Milani P, Gagliardi S, Cova E, Cereda C. SOD1 Transcriptional and Posttranscriptional Regulation and Its Potential Implications in ALS. *Neurol Res Int.* 2011; 2011: 458427.
61. Baldelli S, Aquilano K, Rotilio G, Ciriolo MR. Glutathione and copper, zinc superoxide dismutase are modulated by overexpression of neuronal nitric oxide synthase. *Int J Biochem Cell Biol.* 2008; 40: 2660-70.
62. Bekeschus S, Iseni S, Reuter S, Masur K, Weltmann KD. Nitrogen Shielding of an Argon Plasma Jet and Its Effects on Human Immune Cells. *IEEE Trans Plasma Sci.* 2015; 43: 776-81.
63. Gaens WV, Iseni S, Schmidt-Bleker A, Weltmann KD, Reuter S, Bogaerts A. Numerical analysis of the effect of nitrogen and oxygen admixtures on the chemistry of an argon plasma jet operating at atmospheric pressure. *New J Phys.* 2015; 17: 033003.
64. Iseni S, Reuter S, Weltmann KD. NO₂ dynamics of an Ar/Air plasma jet investigated by in situ quantum cascade laser spectroscopy at atmospheric pressure. *J Phys D: Appl Phys.* 2014; 47: 075203.
65. Tsujii M, Kawano S, Tsuji S, Sawaoka H, Hori M, DuBois RN. Cyclooxygenase regulates angiogenesis induced by colon cancer cells. *Cell.* 1998; 93: 705-16.
66. Nguyen TN, Uemura A, Shih W, Yamada S. Zyxin-mediated actin assembly is required for efficient wound closure. *J Biol Chem.* 2010; 285: 35439-45.
67. Dimmeler S, Zeiher AM. Endothelial cell apoptosis in angiogenesis and vessel regression. *Circ Res.* 2000; 87: 434-9.
68. Carmeliet P, Jain RK. Angiogenesis in cancer and other diseases. *Nature.* 2000; 407.
69. Li L, Pan H, Wang H, Li X, Bu X, Wang Q, et al. Interplay between VEGF and Nrf2 regulates angiogenesis due to intracranial venous hypertension. *Sci Rep.* 2016; 6: 37338.
70. Florzcyk U, Jazwa A, Maleszewska M, Mendel M, Szade K, Kozakowska M, et al. Nrf2 regulates angiogenesis: effect on endothelial cells, bone marrow-derived proangiogenic cells and hind limb ischemia. *Antioxid Redox Signal.* 2014; 20: 1693-708.
71. Uno K, Prow TW, Bhutto IA, Yerrapureddy A, McLeod DS, Yamamoto M, et al. Role of Nrf2 in retinal vascular development and the vaso-obliterative phase of oxygen-induced retinopathy. *Exp Eye Res.* 2010; 90: 493-500.
72. Tan Y, Ichikawa T, Li J, Si Q, Yang H, Chen X, et al. Diabetic downregulation of Nrf2 activity via ERK contributes to oxidative stress-induced insulin resistance in cardiac cells in vitro and in vivo. *Diabetes.* 2011; 60: 625-33.
73. Chen XL, Dodd G, Thomas S, Zhang X, Wasserman MA, Rovin BH, et al. Activation of Nrf2/ARE pathway protects endothelial cells from oxidant injury and inhibits inflammatory gene expression. *Am J Physiol Heart Circ Physiol.* 2006; 290: H1862-70.
74. Arndt S, Schmidt A, Karrer S, von Woedtke T. Comparing two different plasma devices kINPen and Adtec SteriPlas regarding their molecular and cellular effects on wound healing. *Clin Plas Med.* 2018; 9: 24-33.
75. Schmidt A, Bekeschus S. Redox for Repair: Cold Physical Plasmas and Nrf2 Signaling Promoting Wound Healing. *Antioxidants (Basel).* 2018; 7: 146.
76. Valcarcel-Ares MN, Gautam T, Warrington JP, Bailey-Downs L, Sosnowska D, de Cabo R, et al. Disruption of Nrf2 signaling impairs angiogenic capacity of endothelial cells: implications for microvascular aging. *J Gerontol A Biol Sci Med Sci.* 2012; 67: 821-9.
77. Dietz KJ. Redox regulation of transcription factors in plant stress acclimation and development. *Antioxid Redox Signal.* 2014; 21: 1356-72.
78. Rono B, Engelholm LH, Lund LR, Hald A. Gender affects skin wound healing in plasminogen deficient mice. *PLoS One.* 2013; 8: e59942.
79. Mills SJ, Ashworth JJ, Gilliver SC, Hardman MJ, Ashcroft GS. The sex steroid precursor DHEA accelerates cutaneous wound healing via the estrogen receptors. *J Invest Dermatol.* 2005; 125: 1053-62.
80. Ashcroft GS, Dodsworth J, Boxtel EV, Tarnuzzer RW, Horan MA, Schultz GS, et al. Estrogen accelerates cutaneous wound healing associated with an increase in TGF- β 1 levels. *Nat Med.* 1997; 3: 1209-15.
81. Greenhalgh DG, Sprugel KH, Murray MJ, Ross R. PDGF and FGF stimulate wound healing in the genetically diabetic mouse. *Am J Pathol.* 1990; 136: 1235-46.